ACS APPLIED MATERIALS & INTERFACES

www.acsami.org

Research Article

Enhanced Performance of ΔT_{ad} upon Frequent Alternating Magnetic Fields in FeRh Alloys by Introducing Second Phases

Kaiming Qiao, Jianlin Wang, Shulan Zuo, Houbo Zhou, Jiazheng Hao, Yao Liu, Fengxia Hu,* Hu Zhang,* Adler G. Gamzatov,* Akhmed Aliev, Cheng Zhang, Jia Li, Zibing Yu, Yihong Gao, Feiran Shen, Rongchang Ye, Yi Long, Xuedong Bai, Jing Wang,* Jirong Sun, Rongjin Huang, Tongyun Zhao, and Baogen Shen*

Cite This: *ACS Appl. Mater. Interfaces* 2022, 14, 18293−18301

Read Online

ABSTRACT: The cyclability and frequency dependence of the adiabatic temperature change (ΔT_{ad}) under an alternating magnetic field (AMF) are significantly important from the viewpoint of refrigeration application. Our studies demonstrated, by direct measurements, that the cyclability and low-magnetic-field performance of ΔT_{ad} in FeRh alloys can be largely enhanced by introducing second phases. The ΔT_{ad} under a 1.8 T, 0.13 Hz AMF is reduced by 14%, which is much better than that (40−50%) of monophase FeRh previously reported. More importantly, the introduction of second phases enables the antiferromagnetic−ferromagnetic phase transition to be driven by a lower magnetic field. Thus, ΔT_{ad} is significantly enhanced under a 0.62 T, 1 Hz AMF, and its value is 70% larger than that of monophase FeRh previously reported. Although frequency dependence of ΔT_{ad} occurs, the specific cooling power largely increases by 11 times from 0.17 to 1.9 W/g, as the frequency increases from 1 to 18.4 Hz under an AMF of 0.62 T. Our analysis of the phase transition dynamics based on magnetic relaxation measurements indicates that the activation energy barrier is lowered owing to the existence of second phases in FeRh alloys, which should be responsible for the reduction of the driving field. This work provides an effective way to enhance the cyclability and low-magnetic-field performance of ΔT_{ad} under an AMF in FeRh alloys by introducing second phases.

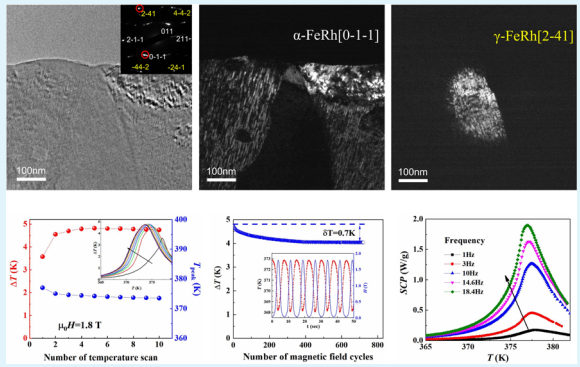

KEYWORDS: *magnetocaloric effect, FeRh, cyclability, adiabatic temperature change, alternating magnetic field*

1. INTRODUCTION

With global warming intensifying, the environmental problems caused by traditional gas-compression refrigeration technology have attracted widespread attention. Especially since the Paris Convention, finding an alternative has become a focal issue. In view of energy-saving and environmentally friendly considerations, magnetic refrigeration is a promising refrigeration technology.[1−13] In magnetic refrigeration devices, the specific cooling power (SCP), which is the cooling power per unit mass or unit volume of the cooling material, is one of the most important metrics for magnetocaloric materials.[7] The larger the SCP, the higher the cooling efficiency. To obtain a large SCP, magnetocaloric materials with large adiabatic temperature changes (ΔT_{ad}) and isothermal entropy changes (ΔS_T) under small magnetic-field changes must be found.[12,13] The magnetocaloric materials with first-order phase transitions have been extensively studied in the past 2 decades due to their large ΔS_T, which have become one of the potential candidate materials in magnetic refrigeration.[10] As a typical first-order phase transition material, the FeRh alloy has attracted much attention due to its superiorities in large adiabatic temperature changes (ΔT_{ad} = 9 K under a magnetic field change of 0−1.8 T[14]) and excellent mechanical properties. Specifically, FeRh alloys were studied and successfully fabricated into nano-scale materials, such as thin films and nanoparticles[15−17] while the first-order phase transition and good magnetocaloric properties were retained. This gives FeRh alloys great potential in some specific application scenarios, such as micro- or nano-scale refrigeration devices. When magnetocaloric materials are used in magnetic refrigeration devices, they must be capable of operating millions of magnetic field cycles.[18] For materials with first-order phase transition, an excellent magnetocaloric effect (MCE) only occurs in the first several magnetic field

Received: December 2, 2021
Accepted: April 1, 2022
Published: April 14, 2022

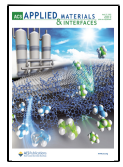

https://doi.org/10.1021/acsami.1c23313
ACS Appl. Mater. Interfaces 2022, 14, 18293−18301

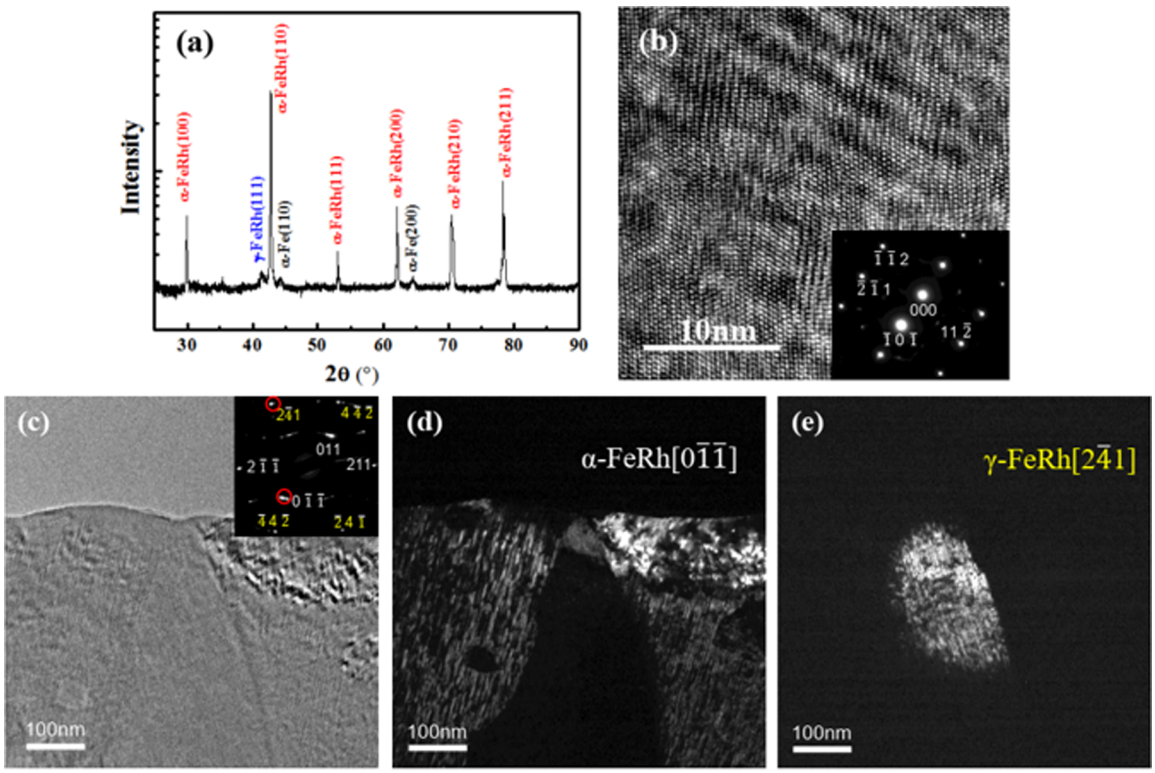

Figure 1. (a) XRD pattern of FeRh bulks at room temperature. (b) High-resolution TEM image of the α-FeRh phase along the [1$\bar{3}$$\bar{1}$] zone axis. (c) TEM image at the position of phase boundaries for α-FeRh. The inset shows the corresponding selected area electron diffraction (SAED) pattern. (d,e) Dark-field TEM images recorded from the same region as (c), where the diffraction spots of (d) α-FeRh [0$\bar{1}$ $\bar{1}$] and (e) γ-FeRh [2$\bar{4}$ 1] are allowed to pass through the hollow objective apertures.

applications, and a large decrease usually occurs for more magnetic field cycling.[14,19,20] The reduction of ΔT_{ad} in the FeRh alloy reaches ∼40−50%.[14] Furthermore, a large magnetic field is usually needed to drive the phase transition in magnetocaloric materials,[21] while a magnet with a high magnetic field is expensive. To use the magnet as efficiently as possible, a high operating frequency is desired,[22] which results in a requirement for magnetocaloric materials to preserve a good performance at a high frequency and a low alternating magnetic field (AMF). Therefore, seeking an effective solution to enhance the cyclability and high-frequency performance of the MCE at low magnetic fields for first-order phase transition materials is urgent. Previously, the MCE in most research studies was mainly characterized by the indirect method, that is, calculating the entropy change based on the Maxwell relationship. In this way, it is difficult to characterize MCE evolution with magnetic field cycles at a high frequency.

In this study, the cyclability and high-frequency performance of the MCE were studied by direct measurements, and we demonstrated that the MCE performance in FeRh alloys is enhanced due to the existence of second phases. The results indicate that not only can the cyclability of ΔT_{ad} in FeRh alloys be enhanced under both temperature and magnetic field cycling but also the driving field of the antiferromagnetic (AFM) to ferromagnetic (FM) phase transition in FeRh alloys is lowered by introducing second phases. Thus, enhancement and frequency dependency of ΔT_{ad} occur under an AMF of 0.62 T, and the deduced SCP increases with the increasing frequency. An analysis of the dynamics of the phase transition demonstrates that a small activation energy barrier and a large relaxation time should be responsible for the reduction of the driving field and frequency dependence of the MCE in FeRh alloys with second phases. This work provides direct experimental support for enhancing the cyclability and low-magnetic-field performance of ΔT_{ad} in FeRh alloys by introducing second phases.

2. EXPERIMENTAL SECTION

An $Fe_{50}Rh_{50}$ (FeRh) alloy ingot with a nominal composition was prepared by arc melting. After melting, the ingot wrapped with molybdenum was sealed in a quartz tube filled with Ar. Then, the ingot was annealed at 1100 °C for 2 weeks and quenched in liquid nitrogen. The obtained FeRh alloy was cut into slices with sizes of 3 × 3 × 0.4 mm^3. The crystal structure of the FeRh alloy was measured by X-ray diffraction (XRD) with a Smart Lab diffractometer using Cu Kα radiation. The room temperature XRD patterns were collected on a bulk slice sample since FeRh alloys are difficult to crack. The XRD patterns were refined using the GSAS/EXPGUI package. The microstructure and the magnetic domain configuration were characterized by conventional transmission electron microscopy (TEM) (JEOL, JEM-2010F) and JEOL-dedicated Lorentz TEM (2100F) with almost no remnant magnetic field around the sample, respectively. The samples for the TEM analyses were first cut from the polycrystalline FeRh ingot by wire-electrode cutting. Then, the FeRh slice was thinned by mechanical polishing, dimpling, and argon ion milling. The magnetic properties were measured using a superconducting quantum interference device (SQUID) magnetometer. The MCE was directly measured by devices manufactured by the Amirkhanov Institute of Physics of Dagestan Scientific Center.[19−21] The AMF was provided by utilizing a linear actuator with a frequency of 0.13 Hz to move the sample into or out of the magnet system. The temperature change in cyclic magnetic fields was measured using a thermocouple made of constantan and chromel wires with a diameter of 25 μm. The ends of the wires were preliminarily flattened up to 3−4 μm in thickness to reduce the thermal inertia of the thermocouple.

https://doi.org/10.1021/acsami.1c23313
ACS Appl. Mater. Interfaces 2022, 14, 18293−18301

To obtain the temporal profiles of the MCE, the temperature evolution profiles of the FeRh alloy were measured by connecting the differential thermocouple output to a Keithley 2000 multimeter. To study the frequency-dependent MCE, a magnetic field source that involved rotating a disk with four permanent magnets of 0.62 T via a stepper motor was used. The frequency of the magnetic field could reach 50 Hz. To avoid the frequency-induced thermal inertia effect in thermocouples, ΔT_{ad} was measured with a maximum frequency of 18.4 Hz.

3. RESULTS AND DISCUSSION

3.1. Structural Properties. Figure 1a shows the XRD pattern of FeRh alloys at room temperature. From this figure, we can clearly see that the α-FeRh phase is dominant, while a small number of second phases (α-Fe phase and γ-FeRh phase) co-exist, which plays an important role in the phase transition of FeRh alloys.[23] From the XRD refinement results (see Supporting Information S1), the total content of the second phases was determined to be 7%, that is, 4.6% α-Fe and 2.4% γ-FeRh phase. To investigate the co-existence of second phases in FeRh alloys, high-resolution TEM characterization and dark-field TEM images were characterized (Figure 1). The main phase of α-FeRh is confirmed in the current FeRh alloys by the high-resolution TEM image shown in Figure 1b. The dark-field TEM technique is an effective and frequently used way to determine the co-existence of multiphase structures or orientations of samples. During the collection of dark-field images, only a certain diffracted beam is allowed to pass through the objective aperture. In the area that meets the Bragg diffraction condition of the diffracted beam selected for imaging, the intensity of the diffracted beam is relatively high, whereby the contrast in the dark-field image is bright. Conversely, the contrast in the image is dark. In this study, dark-field images were obtained at the position of phase boundaries, as shown in Figure 1c. The co-existence of α-FeRh along the $[0\bar{1}1]$ zone axis and γ-FeRh along the [322] zone axis at this position is confirmed by the SAED pattern in the inset of Figure 1c, where the indices of diffraction spots of α-FeRh and γ-FeRh phases are indicated by white and yellow fonts, respectively. The diffracted beams of $[0\bar{1}\,\bar{1}]$ and $[2\bar{4}1]$ are selected for dark-field imaging of α-FeRh and γ-FeRh, respectively. The results are shown in Figure 1d,e. By comparing the two dark-field images (Figure 1d,e), we can clearly see that the γ-FeRh phase with a size of approximately 100−200 nm develops between the two α-FeRh phase boundaries. All the results above demonstrate the presence of second phases in this FeRh alloy. The introduction of second phases will affect the phase transition and MCE of α-FeRh.[23]

3.2. Magnetic Properties. To investigate the effect of the second phases on the phase transition of FeRh alloys, the $M-T$ curves with magnetic fields of 0.4, 2, and 5 T were measured, as shown in Figure 2a. It can be clearly seen that the AFM−FM phase transition with a thermal hysteresis width (approximately 10 K) occurs in the present FeRh alloy. The transition temperature (T_t) determined from the peak value of the $dM/dT-T$ curve (inset of Figure 2a) in the heating process under a magnetic field of 2 T is 370 K. As the magnetic field increases, the transition temperature almost linearly moves to a lower temperature at a rate of 8 K/T (see Supporting Information S2). Thus, the phase transition temperature at the zero magnetic field can be determined to be 386 K by linear extrapolation, which is higher than that of

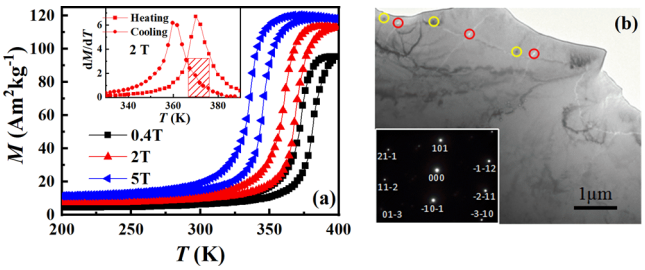

Figure 2. (a) Temperature dependence of magnetization ($M-T$) at magnetic fields of 0.4, 2, and 5 T for FeRh alloys. The inset shows the $dM/dT-T$ curves in the heating process under a magnetic field of 2 T. (b) Under-focused Lorentz TEM image at room temperature. The inset at the left corner shows the SAED pattern along the $[1\bar{3}\,\bar{1}]$ zone axis of the α-FeRh phase. The yellow and red circles mark the opposite chirality vortices with dark and bright contrasts, respectively.

monophase FeRh alloys with the same nominal composition in previous refs 24 and 25. In addition, the full-width (~11 K) at half-maximum of the $dM/dT-T$ curve, as shown in the inset of Figure 2a, is larger than that in the literature,[23,24] indicating a broadened phase transition in FeRh alloys with second phases. The higher transition temperature and broadened phase transition can be attributed to the introduction of the second phases. Although no chemical composition gradients are generated on a large scale at the boundaries of α-FeRh and γ-FeRh phases, stress fields at the boundaries must be considered owing to the differential expansion of the multiphases.[23] The stress fields generated by the second phases can be equal to the hydrostatic pressure. The AFM−FM phase transition in α-FeRh is sensitive to stress, and a compressive (tensile) stress stabilizes the AFM(FM) phase.[15,16] Therefore, the introduction of second phases leads to a higher transition temperature. In addition, the content of the second phases in this study is small, which may lead to a gradient distribution of stress fields close to and far from the second phases, resulting in a broadened phase transition temperature span. Thus, the MCE of FeRh alloys will also be affected (see Supporting Information S3). Furthermore, a small amount of the FM background signal appears in the low-temperature AFM phase, which may come from the α-Fe phase and/or α-FeRh phase. To confirm that the FM signal partially originates from the α-FeRh phase, Lorentz TEM at room temperature was performed, and the result is shown in Figure 2b. The inset at the left corner shows the SAED pattern along the $[1\bar{3}\,\bar{1}]$ axis of the α-FeRh phase. In the upper right corner of Figure 2b, an FM domain with several vortices formed at the domain wall was detected. The yellow and red circles mark the opposite chirality vortices with dark and bright contrast, respectively. The relative origin of the low-temperature FM signal in the α-FeRh phase may be ascribed to the imperfect crystal quality, defects, and strains, which have been previously studied in film samples.[26−29]

3.3. Cyclability of ΔT_{ad}. To clarify the effect of the second phase on the cyclability of the MCE in FeRh alloys, the temperature dependencies of the MCE for FeRh alloys in cyclic magnetic fields were measured. The temperature oscillations were measured by constantan−chromel thermocouples. Their signals first passed through the SR554 transformer preamplifier and were then measured using the SR830 lock-in amplifier.[14] Measurements were made with the continuous application of cyclic magnetic fields at a slow rate of temperature change in the sample. In this study, the

https://doi.org/10.1021/acsami.1c23313
ACS Appl. Mater. Interfaces 2022, 14, 18293−18301

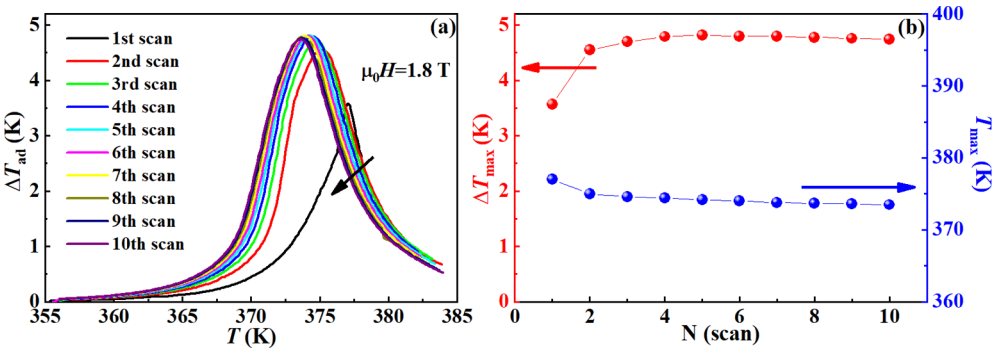

Figure 3. (a) Temperature dependence of adiabatic temperature change ($\Delta T_{ad}-T$) curves over 10 temperature cycles under an AMF of 1.8 T with a frequency of 0.13 Hz; the temperature sweeping speed is 0.5 K/min. (b) ΔT_{max} and its peak position with the number of cycles N. Red and blue arrows are drawn to indicate ΔT_{ad} and its peak position, respectively.

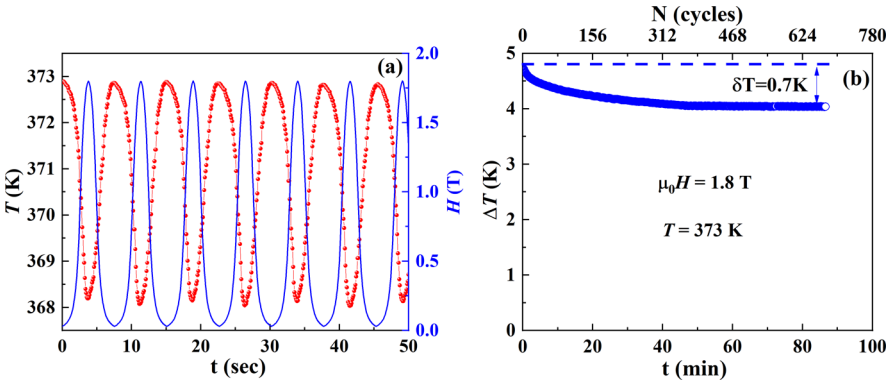

Figure 4. (a) Temperature of FeRh alloys and the AMF as a function of time at T = 373 K. (b) Evolution of ΔT_{ad} with time (bottom x axis) and number of magnetic field cycles (upper x axis) for FeRh alloys at 373 K under a 1.8 T, 0.13 Hz AMF.

temperature dependence of adiabatic temperature change ($\Delta T_{ad}-T$) curves in the heating process was measured for 10 cycles under an AMF of 1.8 T with a frequency of 0.13 Hz, where the temperature sweeping speed was 0.5 K/min. The results are shown in Figure 3a. To clearly describe the influence of temperature cycles on the ΔT_{ad} of FeRh alloys, the evolution of peak values (ΔT_{max}) and peak positions (T_{peak}) with the number of temperature cycles (N) is plotted in Figure 3b. From this figure, we can clearly see that as N increases, the ΔT_{max} of the FeRh alloys first increases and then gradually stabilizes. The largest difference in ΔT_{max} occurs between the first and second temperature cycles, reaching ∼1 K. In the subsequent temperature cycles, the increase in ΔT_{max} decreases. At the fifth temperature cycle, ΔT_{max} reaches the maximum value, and ΔT_{max} remains almost unchanged with a further increase in N. As N increases, the T_{peak} shifts to a lower temperature and then gradually stabilizes. In the first temperature cycle, T_{peak} is approximately 377 K, the same as the peak position in the $\Delta S-T$ curve under 0−2 T (Supporting Information S3), which indirectly proves the reliability of our direct measurements of ΔT_{ad}. The largest movement of T_{peak} appears between the first and second cycles, attaining ∼2 K. As the number of cycles N increases, the movement of T_{peak} gradually slows down and stabilizes. The evolution of ΔT_{max} and T_{peak} with N can be attributed to the combined effect of the suppression of the high-temperature FM phase and motions of AFM and FM domain walls in FeRh alloys. The AFM and FM domain wall motions are mainly caused by magnetic field cycles. Therefore, they should not be the main factor affecting the temperature cyclability of the MCE. The suppressed FM phase with a larger lattice parameter hinders the AFM−FM phase transition and does not undergo a phase transition, which makes the FeRh alloy have a higher transition temperature and a lower ΔT_{max} in the first temperature cycle. As the number of temperature cycles increases under the AMF, the suppressed FM phase gradually transforms into the AFM phase due to the FM−AFM phase transition in the cooling process,[30,31] resulting in the increase in ΔT_{max} and the movement of T_{peak} to a lower temperature with the increase in N. The suppressed FM phase fades away after several temperature cycles. Therefore, the increase in the ΔT_{max} of the FeRh alloys and the movement of T_{peak} are gradually stabilized.

In addition to temperature cycling, magnetic field cycling also influences the MCE of FeRh alloys. To investigate the cyclability under magnetic field cycling, the temperature evolution under AMF cycling of FeRh alloys was determined, and the temperature of FeRh alloys and the normalized magnetic field as a function of time at T = 373 K for the first several magnetic field cycles are representatively shown in Figure 4a. To clearly show the cyclability of the MCE under an AMF, the evolution of ΔT_{ad} for FeRh alloys under a 1.8 T, 0.13 Hz AMF is summarized in Figure 4b. Obviously, as the number of AMF cycles increases, ΔT_{ad} first decreases and then gradually stabilizes. The degradation of ΔT_{ad} is mainly caused by the motion of FM and AFM domain walls under the AMF.[14] The initial ΔT_{ad} under an AMF of 1.8 T is 4.8 K. From Table 1, one can see that the virgin value of ΔT_{ad} of our FeRh alloys is larger than that of most other typical magnetocaloric materials.

https://doi.org/10.1021/acsami.1c23313
ACS Appl. Mater. Interfaces 2022, 14, 18293−18301

Table 1. Comparison of ΔT_{ad} for Typical Magnetocaloric Materials

materials	magnetic field (T)	ΔT_{ad}	references
$Fe_{50}Rh_{50}$	1.8	4.8 K (virgin)	this work
$Fe_{50}Rh_{50}$	1.8	4.1 K (stabilized)	this work
Gd	1.9	4.5 K	32
$Gd_5Si_2Ge_2$	1.5	3.9 K	33
$La(Fe,Mn,Si)13H_x$	1.9	4.5 K	34
$MnAs1-xP_x$	2	1.5 K	35
$Ni_{47}Mn_{40}Sn_{12.5}Cu_{0.5}$	1.8	1.2 K	36
$Sm_{0.6}Sr_{0.4}MnO_3$	1.8	4.4 K	14
$Fe_{50.4}Rh_{49.6}$	1.8	7.5 K (virgin)	37
$Fe_{50.4}Rh_{49.6}$	1.8	3.5 K (stabilized)	37

Cycling stability of MCE is important for practical applications. After stabilization, the ΔT_{ad} under an AMF of 1.8 T is only reduced by 0.7 K, reaching 4.1 K. This value is comparable to that of the benchmark material Gd. More importantly, the reduction ratio is only about 14%, which is much smaller than that in other publications,[14,37] with a reduction ratio of approximately 40−50%. In addition, ΔT_{ad} did not stabilize after 3000 magnetic field cycles in a previous study,[14] while it stabilized after ∼500 cycles in this study, indicating an enhanced cyclability performance. The introduced second phases play an important role in this phenomenon. The second phase may bring about local stresses and stray magnetic fields acting on the neighboring main phase α-FeRh, which will affect the structure and energy density of the domain walls.[38−40] The energy changes may weaken the motion of domain walls and the role of domain boundary areas, thus producing an enhanced cyclability performance. Therefore, the possibility of enhancing the cyclability under temperature and magnetic field cycling by introducing second phases is demonstrated.

According to the formula SCP = $C\Delta Tf$, the SCP after stabilization can be obtained, where C is the specific heat capacity of the material, ΔT is the adiabatic temperature change of the material, and f is the frequency of the AMF. The calculated SCP for the FeRh alloy with second phases is 0.19 W/g in this study, while the value of 0.16 W/g was obtained for the monophase FeRh alloy in the literature.[37] Thus, the energy savings can be obtained to be 0.03 W/g for FeRh alloys with second phases.

3.4. Phase transition Dynamics and Frequency Dependence of ΔT_{ad}. To study the effect of the second phases on the MCE at higher frequencies for the present FeRh alloys, the frequency-dependent ΔT_{ad} under an AMF of 0.62 T was measured. The results are shown in Figure 5a. To clearly see the evolution of ΔT_{ad} under frequency, the peak value (ΔT_{max}) and peak position (T_{peak}) at every frequency are given in the inset in the left corner. ΔT_{max} reaches 0.48 K under a 0.62 T, 1 Hz AMF, which is approximately 70% larger than that of monophase FeRh alloys.[21] The enhancement of ΔT_{ad} at low magnetic fields can also be ascribed to the introduction of second phases. Under the action of an external magnetic field, the FM nucleus in FeRh alloys grows into an FM domain, and then, further magnetization is realized by displacement of the domain walls.[38−40] Magnetization nuclei are generally generated at the locations of crystal defects, dopants, and so forth. The more defects and dopants there are, the easier the magnetization nucleus is formed. The introduced second phases will become nucleation sites, which makes the magnetization nucleus formation easier. Therefore, the driving field of the AFM−FM phase transition in FeRh alloys is lowered, and thus, the AFM−FM phase transition can be driven by an AMF of 0.62 T. Consequently, the ΔT_{ad} under an AMF of 0.62 T is significantly enhanced.

In addition to the enhancement of ΔT_{ad}, frequency dependence of ΔT_{ad} also occurs, as shown in Figure 5a, which is closely related to the kinetics of the magnetic field-induced AFM−FM phase transition in FeRh alloys. As the frequency increases, the ΔT_{max} of FeRh alloys gradually decreases, and T_{peak} moves to a lower temperature. When the frequency is increased to 18.4 Hz, ΔT_{max} is reduced to 0.28 K. Although ΔT_{max} decreases with frequency, the SCP increases. According to the formula, SCP = $C\Delta Tf$, the frequency-dependent SCP is obtained, as shown in Figure 5b. To clearly show the evolution of the SCP with frequency, the peak value of the SCP versus frequency is given in the inset of Figure 5b. The peak value of the SCP for FeRh alloys under a 1 Hz, 0.62 T AMF is 0.17 W/g. In the literature,[21] the SCP of FeRh alloys without second phases under a 0.62 T, 1 Hz AMF is only 0.10 W/g. Accordingly, the energy savings for the FeRh alloy with second phases reach 0.07 W/g under a 0.62 T, 1 Hz AMF. When the working frequency of the AMF increases to 10 Hz, which is the maximum frequency existing in the present magnetic refrigeration prototypes, the SCP is 1.27 W/g for the FeRh alloy with second phases in the current study and

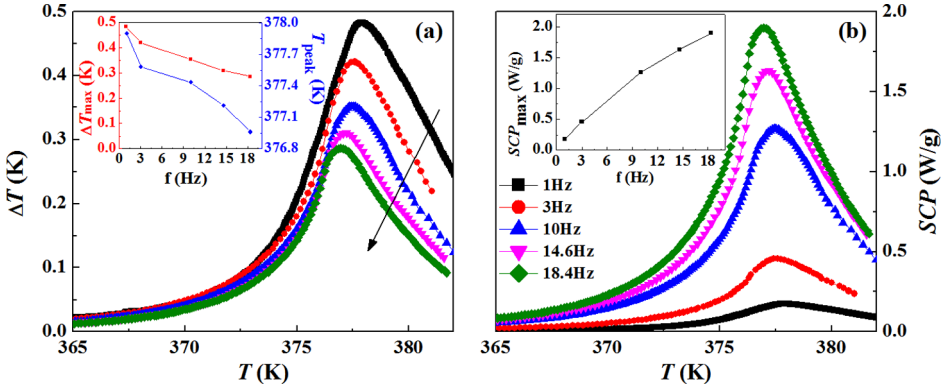

Figure 5. Frequency-dependent (a) ΔT_{ad} and (b) SCP of FeRh alloys under an AMF of 0.62 T; the inset shows the corresponding peak value and peak position at different frequencies.

https://doi.org/10.1021/acsami.1c23313
ACS Appl. Mater. Interfaces 2022, 14, 18293−18301

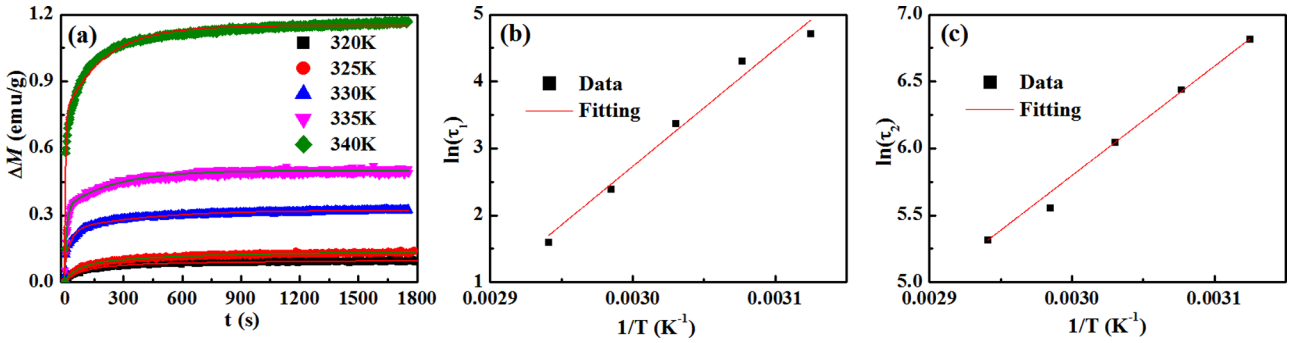

Figure 6. (a) Measured changes in magnetization (symbols) at 4 T and their fitting models (lines) based on eq 1 for five different temperatures. (b,c) Natural logarithm of time constant τ versus $1/T$, confirming the Arrhenius-type thermodynamic relationship with double energy barriers. Symbols are data calculated from eq 1, and lines are the linear fittings of the symbols.

0.90 W/g for that without second phases in the literature.[21] We can see that the energy savings of the FeRh alloys with second phases in the current study under a 0.62 T, 10 Hz AMF reach 0.37 W/g. The SCP reaches 1.90 W/g as the frequency of the AMF increases to 18.4 Hz, which is 11 times larger than that at 1 Hz. This proves that, under the circumstances of satisfying abundant heat exchange, the SCP can be largely improved by raising the operating frequency.

To better understand the frequency dependence of ΔT_{ad}, the dynamics of the magnetic field-induced AFM−FM phase transition in FeRh alloys were investigated by magnetic relaxation measurements. In this way, the relaxation time τ and activation energy barrier ΔE of the magnetic field-induced phase transition can be obtained with a thermal activation model,[41,42] which can quantitatively describe the dynamic process of the magnetic field-induced AFM−FM phase transition.

The time evolution of the magnetization at five typical temperatures was measured as follows. The FeRh alloy was first heated to the target temperature of 100 K and equilibrated for 600 s. Then, the magnetic field was ramped up to 4 T with a maximum speed of 700 Oe/s and held for the duration of the measurement. The magnetization was recorded every 3 s, and the corresponding change in magnetization at five typical temperatures around the phase transition is shown in Figure 6a. The results were then analyzed by an exponential relaxation using eq 1

$$\Delta M(t) = \Delta M(1 - \exp(-t/\tau)) \quad (1)$$

where ΔM is the asymptotic value of $\Delta M(t)$ at 4 T, and τ is the relaxation time. At a definite temperature and magnetic field, the value of the relaxation time τ can be determined in a thermally activated process with a single barrier. However, for the present FeRh sample, the second phases bring about local stresses acting on the neighboring α-FeRh phase, which significantly affects the phase transition and thermally activated process. The α-FeRh phase is far from the second phase and those nearby sustain different stresses; thus, the activation energy barrier of the α-FeRh phase varies from position to position. Therefore, the phase transition activation energy barrier will not be a fixed value in the present FeRh sample but lie in an interval. Two different relaxation times τ were used in the fitting model, and the results are shown in Figure 6. The obtained relaxation time for the FeRh alloy is about 4.9 s at 340 K, which should be responsible for the frequency dependence of the MCE in FeRh alloys under an AMF.

The energy barrier ΔE in the thermally activated process can be determined by eq 2

$$\tau = A/c \exp(\Delta E/kT) \quad (2)$$

where c is the "attempt frequency", and A is a constant. From Figure 6b,c, double energy barriers ΔE_1 and ΔE_2 were obtained, and the barrier heights were 1.54 and 0.72 eV, respectively. Both ΔE_1 and ΔE_2 are smaller than those of $Gd_5(Si,Ge)_4$[41] and $La(Fe,Si)_{13}$[42,43] compounds, which can be ascribed to the introduction of second phases. The second phases become nucleation sites in the AFM−FM phase transition process, making the phase transition easier, and therefore, the phase transition activation energy barrier is significantly reduced. The small energy barrier enables the phase transition of FeRh alloys to be driven by a magnetic field of 0.62 T. Therefore, by introducing second phases, the driving magnetic field of the AFM−FM phase transition in FeRh alloys can be lowered. Thus, ΔT_{ad} is significantly enhanced under an AMF of 0.62 T and frequency dependence of the MCE can be induced.

4. CONCLUSIONS

In conclusion, the cyclability of ΔT_{ad} under an AMF in FeRh alloys has been enhanced by introducing second phases, that is, α-Fe and γ-FeRh, the existence of which is demonstrated by dark-field TEM images. After ∼500 magnetic field cycles of 0−1.8 T at 0.13 Hz, the ΔT_{ad} confirmed by the direct measurement is reduced by about 14% and stabilized, which is much better than that (40−50%) of monophase FeRh previously reported. Moreover, the activation energy barrier in FeRh alloys is lowered by introducing second phases, which is proven by the quantitative calculation of phase transition dynamics. This enables the AFM−FM phase transition in FeRh alloys to be driven by a low magnetic field of 0.62 T. Thus, ΔT_{ad} is significantly enhanced, and frequency dependence occurs under an AMF of 0.62 T at 1 Hz. Although ΔT_{ad} decreases from 0.48 to 0.28 K with the frequency increasing from 1 to 18.4 Hz, the deduced SCP largely increases by 11 times from 0.17 to 1.9 W/g. This research not only offers the possibility to enhance the cyclability and low-field performance of magnetocaloric materials similar to FeRh alloy by utilizing a small number of second phases but also provides direct experimental support for possible application of FeRh alloys in magnetic refrigeration.

https://doi.org/10.1021/acsami.1c23313
ACS Appl. Mater. Interfaces 2022, 14, 18293−18301

■ ASSOCIATED CONTENT

Supporting Information

The Supporting Information is available free of charge at https://pubs.acs.org/doi/10.1021/acsami.1c23313.

MCE of FeRh alloys measured in both indirect and direct methods (PDF)

■ AUTHOR INFORMATION

Corresponding Authors

Fengxia Hu − *Beijing National Laboratory for Condensed Matter Physics, Institute of Physics, Chinese Academy of Sciences, Beijing 100190, P. R. China; School of Physical Sciences, University of Chinese Academy of Sciences, Beijing 100049, P. R. China; Songshan Lake Materials Laboratory, Dongguan, Guangdong 523808, P. R. China;* orcid.org/0000-0003-0383-0213; Email: fxhu@iphy.ac.cn

Hu Zhang − *School of Materials Science and Engineering, University of Science and Technology of Beijing, Beijing 100083, P. R. China;* orcid.org/0000-0001-8726-8605; Email: zhanghu@ustb.edu.cn

Adler G. Gamzatov − *Amirkhanov Institute of Physics of DFRC of RAS, Makhachkala 367003, Russia;* orcid.org/0000-0002-0254-2183; Email: gamzatov_adler@mail.ru

Jing Wang − *Beijing National Laboratory for Condensed Matter Physics, Institute of Physics, Chinese Academy of Sciences, Beijing 100190, P. R. China; School of Physical Sciences, University of Chinese Academy of Sciences, Beijing 100049, P. R. China; Fujian Innovation Academy, Chinese Academy of Sciences, Fuzhou, Fujian 350108, P. R. China;* orcid.org/0000-0001-5458-6711; Email: wangjing@iphy.ac.cn

Baogen Shen − *Beijing National Laboratory for Condensed Matter Physics, Institute of Physics, Chinese Academy of Sciences, Beijing 100190, P. R. China; School of Physical Sciences, University of Chinese Academy of Sciences, Beijing 100049, P. R. China; Ningbo Institute of Materials Technology & Engineering, Chinese Academy of Sciences, Ningbo, Zhejiang 315201, China*; Email: shenbg@iphy.ac.cn

Authors

Kaiming Qiao − *School of Materials Science and Engineering, University of Science and Technology of Beijing, Beijing 100083, P. R. China; Beijing National Laboratory for Condensed Matter Physics, Institute of Physics, Chinese Academy of Sciences, Beijing 100190, P. R. China*

Jianlin Wang − *Beijing National Laboratory for Condensed Matter Physics, Institute of Physics, Chinese Academy of Sciences, Beijing 100190, P. R. China; School of Physical Sciences, University of Chinese Academy of Sciences, Beijing 100049, P. R. China;* orcid.org/0000-0002-1749-4428

Shulan Zuo − *School of Materials Science and Engineering, Beihang University, Beijing 100191, P. R. China*

Houbo Zhou − *Beijing National Laboratory for Condensed Matter Physics, Institute of Physics, Chinese Academy of Sciences, Beijing 100190, P. R. China; School of Physical Sciences, University of Chinese Academy of Sciences, Beijing 100049, P. R. China*

Jiazheng Hao − *Beijing National Laboratory for Condensed Matter Physics, Institute of Physics, Chinese Academy of Sciences, Beijing 100190, P. R. China; School of Physical Sciences, University of Chinese Academy of Sciences, Beijing 100049, P. R. China*

Yao Liu − *Frontier Institute of Science and Technology, State Key Laboratory for Mechanical Behavior of Materials, and MOE Key Laboratory for Nonequilibrium Synthesis and Modulation of Condensed Matter, Xi'an Jiaotong University, Xi'an 710054, P. R. China*

Akhmed Aliev − *Amirkhanov Institute of Physics of DFRC of RAS, Makhachkala 367003, Russia*

Cheng Zhang − *Beijing National Laboratory for Condensed Matter Physics, Institute of Physics, Chinese Academy of Sciences, Beijing 100190, P. R. China; School of Physical Sciences, University of Chinese Academy of Sciences, Beijing 100049, P. R. China*

Jia Li − *Beijing National Laboratory for Condensed Matter Physics, Institute of Physics, Chinese Academy of Sciences, Beijing 100190, P. R. China; School of Physical Sciences, University of Chinese Academy of Sciences, Beijing 100049, P. R. China*

Zibing Yu − *Beijing National Laboratory for Condensed Matter Physics, Institute of Physics, Chinese Academy of Sciences, Beijing 100190, P. R. China; School of Physical Sciences, University of Chinese Academy of Sciences, Beijing 100049, P. R. China*

Yihong Gao − *Beijing National Laboratory for Condensed Matter Physics, Institute of Physics, Chinese Academy of Sciences, Beijing 100190, P. R. China; School of Physical Sciences, University of Chinese Academy of Sciences, Beijing 100049, P. R. China*

Feiran Shen − *Beijing National Laboratory for Condensed Matter Physics, Institute of Physics, Chinese Academy of Sciences, Beijing 100190, P. R. China; School of Physical Sciences, University of Chinese Academy of Sciences, Beijing 100049, P. R. China*

Rongchang Ye − *School of Materials Science and Engineering, University of Science and Technology of Beijing, Beijing 100083, P. R. China*

Yi Long − *School of Materials Science and Engineering, University of Science and Technology of Beijing, Beijing 100083, P. R. China*

Xuedong Bai − *Beijing National Laboratory for Condensed Matter Physics, Institute of Physics, Chinese Academy of Sciences, Beijing 100190, P. R. China; School of Physical Sciences, University of Chinese Academy of Sciences, Beijing 100049, P. R. China; Songshan Lake Materials Laboratory, Dongguan, Guangdong 523808, P. R. China;* orcid.org/0000-0002-1403-491X

Jirong Sun − *Beijing National Laboratory for Condensed Matter Physics, Institute of Physics, Chinese Academy of Sciences, Beijing 100190, P. R. China; School of Physical Sciences, University of Chinese Academy of Sciences, Beijing 100049, P. R. China; Songshan Lake Materials Laboratory, Dongguan, Guangdong 523808, P. R. China*

Rongjin Huang − *Key Laboratory of Cryogenics, Technical Institute of Physics and Chemistry, Chinese Academy of Sciences, Beijing 100190, P. R. China;* orcid.org/0000-0002-8730-153X

Tongyun Zhao − *Beijing National Laboratory for Condensed Matter Physics, Institute of Physics, Chinese Academy of Sciences, Beijing 100190, P. R. China; Ganjiang Innovation Academy, Chinese Academy of Sciences, Ganzhou, Jiangxi 341000, P. R. China*

Complete contact information is available at:
https://pubs.acs.org/10.1021/acsami.1c23313

Author Contributions

F.H. and J.W. conceived the idea and designed the experiments. K.Q. carried out laboratory research on sample preparation, magnetic measurement, and structure measurement and wrote the draft of the article. J.W., X.B., and Y.L. carried out laboratory research of HRTEM and contributed in writing the dark-field image section of the article. S.Z. carried out the laboratory research of LTEM and contributed in writing the magnetic domain structure image section of the article. H.Z. and J.H. helped perform the theoretical research on phase transition dynamics. H.Z. revised the draft of the article. A.G.G. and A.A. carried out the laboratory research of adiabatic temperature change measurement. C.Z., J.L., Z.Y., Y.G., F.S., R.Y., J.S., R.H., T.Z., and Y.L. helped execute the laboratory research and discussed all the results. B.S. supervised the research.

Notes

The authors declare no competing financial interest.

■ ACKNOWLEDGMENTS

This work was supported by the National Key Research and Development Program of China (2019YFA0704900, 2021YFB3501200, 2020YFA0711502, 2018YFA0305704, and 2021YFA1400300); the National Natural Sciences Foundation of China (52088101, U1832219, 51771223, 51971240, 52101210, 52171169, and 51671022); the China Postdoctoral Science Foundation (grant no. 2021M690346); the Strategic Priority Research Program B (XDB33030200), and the key research programs (ZDRW-CN-2021-3, 112111KYSB20180013) of the Chinese Academy of Sciences (CAS); the reported study was also funded by RFBR and NSFC, project number 21-58-53046, 52111530044.

■ REFERENCES

(1) Pecharsky, V. K.; Gschneidner, K. A., Jr. Giant Magnetocaloric Effect in $Gd_5Si_2Ge_2$. *Phys. Rev. Lett.* **1997**, *78*, 4494−4497.
(2) Neese, B.; Chu, B.; Lu, S.-G.; Wang, Y.; Furman, E.; Zhang, Q. M. Large Electrocaloric Effect in Ferroelectric Polymers Near Room Temperature. *Science* **2008**, *321*, 821−823.
(3) Tušek, J.; Engelbrecht, K.; Eriksen, D.; Dall'olio, S.; Tušek, J.; Pryds, N. A Regenerative Elastocaloric Heat Pump. *Nat. Energy* **2016**, *1*, 16134.
(4) Moya, X.; Kar-Narayan, S.; Mathur, N. D. Caloric Materials Near Ferroic Phase Transitions. *Nat. Mater.* **2014**, *13*, 439−450.
(5) Mañosa, L.; Planes, A. Materials with Giant Mechanocaloric Effects: Cooling by Strength. *Adv. Mater.* **2017**, *29*, 1603607.
(6) Tegus, O.; Brück, E.; Buschow, K. H. J.; de Boer, F. R. Transition-metal-based Magnetic Refrigerants for Room-temperature Applications. *Nature* **2002**, *415*, 150−152.
(7) Wu, J.; Lu, B.; Liu, C.; He, J. A novel cascade micro-unit regeneration cycle for solid state magnetic Refrigeration. *Appl. Therm. Eng.* **2018**, *137*, 836−847.
(8) Hu, F.-x.; Shen, B.-g.; Sun, J.-r.; Cheng, Z.-h.; Rao, G.-h.; Zhang, X.-x. Influence of Negative Lattice Expansion and Metamagnetic Transition on Magnetic Entropy Change in the Compound $LaFe_{11.4}Si_{1.6}$. *Appl. Phys. Lett.* **2001**, *78*, 3675−3677.
(9) Fujita, A.; Fujieda, S.; Hasegawa, Y.; Fukamichi, K. Itinerant-electron Metamagnetic Transition and Large Magnetocaloric Effects in $La(Fe_xSi_{1-x})_{13}$ Compounds and Their Hydrides. *Phys. Rev. B: Condens. Matter Mater. Phys.* **2003**, *67*, 104416.
(10) GschneidnerJr, K. A.; Pecharsky, V. K.; Tsokol, A. O. Recent Developments in Magnetocaloric Materials. *Rep. Prog. Phys.* **2005**, *68*, 1479−1539.
(11) Yu, B.; Liu, M.; Egolf, P. W.; Kitanovski, A. A Review of Magnetic Refrigerator and Heat Pump Prototypes Built Before the Year 2010. *Int. J. Refrig.* **2010**, *33*, 1029−1060.
(12) Gottschall, T.; Skokov, K. P.; Fries, M.; Taubel, A.; Radulov, I.; Scheibel, F.; Benke, D.; Riegg, S.; Gutfleisch, O. Making a Cool Choice: The Materials Library of Magnetic Refrigeration. *Adv. Energy Mater.* **2019**, *9*, 1901322.
(13) Kitanovski, A. Energy Applications of Magnetocaloric Materials. *Adv. Energy Mater.* **2020**, *10*, 1903741.
(14) Aliev, A. M.; Batdalov, A. B.; Khanov, L. N.; Kamantsev, A. P.; Koledov, V. V.; Mashirov, A. V.; Shavrov, V. G.; Grechishkin, R. M.; Kaul, A. R.; Sampath, V. Reversible Magnetocaloric Effect in Materials With First Order Phase Transitions in Cyclic Magnetic Fields: $Fe_{48}Rh_{52}$ and $Sm_{0.6}Sr_{0.4}MnO_3$. *Appl. Phys. Lett.* **2016**, *109*, 202407.
(15) Qiao, K.; Hu, F.; Liu, Y.; Li, J.; Kuang, H.; Zhang, H.; Liang, W.; Wang, J.; Sun, J.; Shen, B. Novel Reduction of Hysteresis Loss Controlled by Strain Memory Effect in FeRh/PMN-PT Heterostructures. *Nano Energy* **2019**, *59*, 285−294.
(16) Qiao, K.; Wang, J.; Hu, F.; Li, J.; Zhang, C.; Liu, Y.; Yu, Z.; Gao, Y.; Su, J.; Shen, F.; Zhou, H.; Bai, X.; Wang, J.; Franco, V.; Sun, J.; Shen, B. Regulation of Phase Transition and Magnetocaloric Effect by Ferroelectric Domains in FeRh/PMN-PT Heterojunctions. *Acta Mater.* **2020**, *191*, 51−59.
(17) Qiao, K.; Liang, Y.; Zhang, H.; Hu, F.; Yu, Z.; Long, Y.; Wang, J.; Sun, J.; Zhao, T.; Shen, B. Manipulation of magnetocaloric effect in FeRh films by epitaxial growth. *J. Alloys Compd.* **2022**, *907*, 164574.
(18) Lyubina, J.; Schäfer, R.; Martin, N.; Schultz, L.; Gutfleisch, O. Novel Design of $La(Fe,Si)_{13}$ Alloys Towards High Magnetic Refrigeration Performance. *Adv. Mater.* **2010**, *22*, 3735−3739.
(19) Chirkova, A.; Skokov, K. P.; Schultz, L.; Baranov, N. V.; Gutfleisch, O.; Woodcock, T. G. Giant Adiabatic Temperature Change in FeRh Alloys Evidenced by Direct Measurements Under Cyclic Conditions. *Acta Mater.* **2016**, *106*, 15−21.
(20) Stern-Taulats, E.; Gràcia-Condal, A.; Planes, A.; Lloveras, P.; Barrio, M.; Tamarit, J.-L.; Pramanick, S.; Majumdar, S.; Mañosa, L. Reversible Adiabatic Temperature Changes at The Magnetocaloric And Barocaloric Effects in $Fe_{49}Rh_{51}$. *Appl. Phys. Lett.* **2015**, *107*, 152409.
(21) Aliev, A. M.; Batdalov, A. B.; Khanov, L. N.; Koledov, V. V.; Shavrov, V. G.; Tereshina, I. S.; Taskaev, S. V. Magnetocaloric Effect in Some Magnetic Materials in Alternating Magnetic Fields Up To 22 Hz. *J. Alloys Compd.* **2016**, *676*, 601−605.
(22) Bjørk, R.; Bahl, C. R. H.; Nielsen, K. K. The lifetime cost of a magnetic refrigerator. *Int. J. Refrig.* **2016**, *63*, 48−62.
(23) Chirkova, A.; Bittner, F.; Nenkov, K.; Baranov, N. V.; Schultz, L.; Nielsch, K.; Woodcock, T. G. The Effect of the Microstructure on the Antiferromagnetic To Ferromagnetic Transition in FeRh Alloys. *Acta Mater.* **2017**, *131*, 31−38.
(24) Komlev, A. S.; Karpenkov, D. Y.; Gimaev, R. R.; Chirkova, A.; Akiyama, A.; Miyanaga, T.; Hupalo, M. F.; Aguiar, D. J. M.; Carvalho, A. M. G.; Jiménez, M. J.; Cabeza, G. F.; Zverev, V. I.; Perov, N. S. Correlation between magnetic and crystal structural sublattices in palladium-doped FeRh alloys: Analysis of the metamagnetic phase transition driving forces. *J. Alloys Compd.* **2022**, *898*, 163092.
(25) Arreguín-Hernández, M. L.; Sánchez-Valdés, C. F.; Llamazares, J. L. S.; Ríos-Jara, D.; Pecharsky, V. K.; Blinov, M. I.; Prudnikov, V. N.; Kovalev, B. B.; Zverev, V. I.; Tishin, A. M. Magnetoelastic transition and magnetocaloric effect in induction melted $Fe_{100-x}Rh_x$ bulk alloys with x = 50, 51. *J. Alloys Compd.* **2021**, *871*, 159586.
(26) Fan, R.; Kinane, C. J.; Charlton, T. R.; Dorner, R.; Ali, M.; de Vries, M. A.; Brydson, R. M. D.; Marrows, C. H.; Hickey, B. J.; Arena, D. A.; Tanner, B. K.; Nisbet, G.; Langridge, S. Ferromagnetism at the Interfaces of Antiferromagnetic FeRh Epilayers. *Phys. Rev. B: Condens. Matter Mater. Phys.* **2010**, *82*, 184418.
(27) Han, G. C.; Qiu, J. J.; Yap, Q. J.; Luo, P.; Kanbe, T.; Shige, T.; Laughlin, D. E.; Zhu, J.-G. Suppression of Low-temperature

Ferromagnetic Phase in Ultrathin FeRh Films. *J. Appl. Phys.* **2013**, *113*, 123909.
(28) Han, G. C.; Qiu, J. J.; Yap, Q. J.; Luo, P.; Laughlin, D. E.; Zhu, J. G.; Kanbe, T.; Shige, T. Magnetic Stability of Ultrathin FeRh Films. *J. Appl. Phys.* **2013**, *113*, 17C107.
(29) Loving, M.; Jimenez-Villacorta, F.; Kaeswurm, B.; Arena, D. A.; Marrows, C. H.; Lewis, L. H. Structural Evidence For Stabilized Ferromagnetism in Epitaxial FeRh Nanoislands. *J. Phys. D* **2013**, *46*, 162002.
(30) Ko, H. Y. Y.; Suzuki, T.; Phuoc, N. N.; Cao, J. Fabrication and Characterization of FeRh Nanoparticles. *J. Appl. Phys.* **2008**, *103*, 07D508.
(31) Lewis, L. H.; Marrows, C. H.; Langridge, S. Coupled Magnetic, Structural, and Electronic Phase Transitions in FeRh. *Journal of Physics D Applied Physics* **2016**, *49*, 323002.
(32) Dan'kov, S. Y.; Tishin, A. M.; Pecharsky, V. K.; GschneidnerJr, K. A. Magnetic phase transitions and the magnetothermal properties of gadolinium. *Phys. Rev. B: Condens. Matter Mater. Phys.* **1998**, *57*, 3478.
(33) Zeng, H.; Kuang, C.; Zhang, J.; Yue, M. Magnetocaloric effect of $Gd_5Si_2Ge_2$ alloys in low magnetic field. *Bull. Mater. Sci.* **2011**, *34*, 825−828.
(34) Radulov, I. A.; Skokov, K. P.; Karpenkov, D. Y.; Gottschall, T.; Gutfleisch, O. On the preparation of $La(Fe,Mn,Si)_{13}H_x$ polymer-composites with optimized magnetocaloric properties. *J. Magn. Magn. Mater.* **2015**, *396*, 228−236.
(35) Aliev, A. M.; Khanov, L. N.; Gamzatov, A. G.; Batdalov, A. B.; Kurbanova, D. R.; Yanushkevich, K. I.; Govor, G. A. Giant Magnetocaloric Effect in $MnAs_{1-x}P_x$ in A Cyclic Magnetic Field: Lattice and Magnetic Contributions and Degradation of the Effect. *Appl. Phys. Lett.* **2021**, *118*, 072404.
(36) Gamzatov, A. G.; Aliev, A. M.; Ghotbi Varzaneh, A.; Kameli, P.; Abdolhosseini Sarsari, I.; Yu, S. C. Inverse-direct Magnetocaloric Effect Crossover in $Ni_{47}Mn_{40}Sn_{12.5}Cu_{0.5}$ Heusler Alloy in Cyclic Magnetic Fields. *Appl. Phys. Lett.* **2018**, *113*, 172406.
(37) Zverev, V. I.; Saletsky, A. M.; Gimaev, R. R.; Tishin, A. M.; Miyanaga, T.; Staunton, J. B. Influence of structural defects on the magnetocaloric effect in the vicinity of the first order magnetic transition in $Fe_{50.4}Rh_{49.6}$. *Appl. Phys. Lett.* **2016**, *108*, 192405.
(38) Khaykovich, B.; Zeldov, E.; Majer, D.; Li, T. W.; Kes, P. H.; Konczykowski, M. Vortex-Lattice Phase Transitions in $Bi_2Sr_2CaCu_2O_8$ Crystals with Different Oxygen Stoichiometry. *Phys. Rev. Lett.* **1996**, *76*, 2555−2558.
(39) Chang, K.; Feng, W.; Chen, L.-Q. Effect of Second-phase Particle Porphology on Grain Growth Kinetics. *Acta Mater.* **2009**, *57*, 5229−5236.
(40) Tang, X.; Li, J.; Sepehri-Amin, H.; Ohkubo, T.; Hioki, K.; Hattori, A.; Hono, K. Improved Coercivity and Squareness in Bulk Hot-deformed Nd−Fe−B Magnets by Two-step Eutectic Grain Boundary Diffusion Process. *Acta Mater.* **2021**, *203*, 116479.
(41) Leib, J.; Snyder, J. E.; Lograsso, T. A.; Schlagel, D.; Jiles, D. C. Dynamics of the Magnetic Field-induced First Order Magnetic-structural Phase Transformation of $Gd_5(Si_{0.5}Ge_{0.5})_4$. *J. Appl. Phys.* **2004**, *95*, 6915−6917.
(42) Zhang, H.-w.; Wang, F.; Zhao, T.-y.; Zhang, S.-y.; Sun, J.-r.; Shen, B.-g. Thermally Activated Itinerant Metamagnetic Transition in $LaFe_{11.7}Si_{1.3}$. *Phys. Rev. B: Condens. Matter Mater. Phys.* **2004**, *70*, 212402.
(43) Lovell, E.; Pereira, A. M.; Caplin, A. D.; Lyubina, J.; Cohen, L. F. Dynamics of the First-Order Metamagnetic Transition in Magnetocaloric $La(Fe,Si)_{13}$: Reducing Hysteresis. *Adv. Energy Mater.* **2015**, *5*, 1401639.

https://doi.org/10.1021/acsami.1c23313
ACS Appl. Mater. Interfaces 2022, 14, 18293−18301